Modeling Flood Risk Communication and Evacuation Dynamics Using an Agent-Based Framework: A Cedar Rapids, Iowa Case Study

S M Samiul Islam[1,2*], Ibrahim Demir[3,4]

[1] IIHR Hydroscience and Engineering, University of Iowa, Iowa City, 52242, US.
[2] Civil and Environmental Engineering, University of Iowa, Iowa City, US.
[3] River-Coastal Science and Engineering, Tulane University, LA, USA
[4] ByWater Institute, Tulane University
[*]Corresponding author

Abstract

The benefits of effective flood-risk communication in urban river basins are reliant upon the timing of warnings with respect to flood evolution and challenges encountered by vulnerable populations. However, these benefits can reduce losses substantially. This study presents a geospatial agent-based model of flood evacuation for Cedar Rapids, Iowa. The model accounts for stage-specific flood inundation scenarios, road accessibility, evacuation locations and capacities, and heterogeneous household behavior. Evacuation outcomes were assessed across three flood stages, which represent onset (pre-peak), peak (crest), and recession (post-peak) conditions. The warning delays were 0, 2, 4, and 6 hours. The model generates a normalized economic loss index, final evacuation completion success, and evacuation trajectories over time. In the onset stage, the ultimate evacuation is reduced from approximately 57% to 39% (overall) and from 38% to 25% (vulnerable) when warnings are delayed from 0 to 6 hours. This delay results in a concurrent increase in loss from approximately 0.28 to 0.36. The results demonstrate a strong stage dependence. Although evacuation completion remains at nearly 99% across delays during the summit stage, losses increase from approximately 0.33 to 0.38, highlighting the significance of timing-dependent exposure even when evacuation is nearly complete. A persistent vulnerable deficiency of 10–12 percent is observed during the recession stage, with outcomes that are essentially delay-insensitive (overall 94–95%, vulnerable 82–83%, loss 0.30–0.31). These results underscore the necessity of tailored mobility and shelter-access interventions to mitigate persistent inequities in evacuation outcomes and support stage-aware warning strategies.

Keywords: flood evacuation; agent-based model; GIS; warning delay; vulnerable populations; shelter capacity; road accessibility.

1. Introduction

Flooding remains the most widespread and damaging natural hazard worldwide, accounting for more than 40 percent of all recorded natural disasters and affecting an average of 250 million people each year (IPCC, 2022; UNISDR, 2015). Within the United States, flood losses have steadily increased over the past several decades due to rapid urbanization, climate variability, and encroachment of infrastructure into flood-prone zones (Milly et al., 2008; Wing et al., 2022; Alabbad et al., 2024). The U.S. Midwest is particularly vulnerable because of its large river systems, intense convective rainfall patterns, and extensive agricultural and urban land use (Grant et al., 2024; Alabbad and Demir, 2024). The Cedar River Basin of eastern Iowa represents one of the region's most flood-affected catchments, experiencing multiple major floods in 1993, 2008, and 2016 (Eash, 2015; FEMA, 2010). The June 2008 flood in Cedar Rapids, in particular, caused catastrophic damage, submerging more than ten square miles of the city, displacing over 10,000 residents, and resulting in economic losses exceeding six billion U.S. dollars (City of Cedar Rapids, 2011). Despite substantial advances in hydrologic forecasting and floodplain management (Sajja et al., 2025), the disaster underscored a persistent challenge in flood risk reduction: even when accurate warnings are issued, many residents fail to evacuate in time due to behavioral, informational, and logistical barriers (Lindell & Perry, 2012; Morss et al., 2016; Islam & Demir, 2025).

Flood-risk management has traditionally emphasized structural defenses, such as levees, detention basins, and floodwalls, along with hydrologic and hydraulic modeling for hazard prediction (Merz et al., 2010; Pappenberger et al., 2015). However, a growing body of research highlights that the effectiveness of early warning systems depends not only on technical accuracy but also on the social dynamics of information communication, perception, and trust (Kox & Thieken, 2017; Morss et al., 2017; Rufat et al., 2020; Baydaroğlu et al., 2023). Behavioral and social factors, such as credibility of the message source, prior flood experience, peer influence, and perceived controllability, play a decisive role in determining whether individuals translate information into protective action (Lindell & Perry, 2012; Mileti & Peek, 2000). Studies of the 2008 Midwest floods and subsequent events revealed that delays in warning dissemination, misinformation on social media, and a lack of trust in institutional authorities substantially reduced compliance with evacuation orders (Dash & Gladwin, 2007; Paul & Dutt, 2010). Consequently, there is a growing recognition that the human behavioral response is often the weakest link in the risk communication chain (Solberg et al., 2010; Wachinger et al., 2013; Yesilkoy et al., 2024).

The trust component of flood communication has been extensively discussed in the risk perception literature (Islam & Demir, 2026). Trust is conceptualized as the belief that the warning source is credible, competent, and acting in the public's interest (Siegrist & Cvetkovich, 2000; Slovic, 1993). Low trust can amplify uncertainty and lead to noncompliance, even when hazard information is technically accurate (Terpstra et al., 2009). Conversely, high trust can compensate for incomplete information and foster coordinated protective behavior across a community (Paton, 2008). Trust is therefore an essential mediating variable in behavioral decision-making frameworks such as the Protective Action Decision Model (PADM) (Lindell & Perry, 2012) and

the Social Amplification of Risk Framework (SARF) (Kasperson et al., 1988). These theories emphasize that warnings do not affect individuals directly but rather through a series of social and cognitive filters, including credibility appraisal, social confirmation, and perceived efficacy of action.

Parallel to these advances in behavioral theory, Agent-Based Models (ABMs) have emerged as powerful tools for simulating collective human behavior in dynamic hazard contexts (Crooks & Heppenstall, 2012; Dawson et al., 2011; Haer et al., 2016). Unlike traditional aggregate evacuation models, ABMs represent each individual as an autonomous "agent" capable of perceiving risk, making decisions, and interacting with other agents and the environment (Kadiyala et al., 2025). This allows emergent phenomena, such as delayed evacuations, clustered decision-making, or network-driven cascades of awareness (Demiray et al., 2025), to be explored explicitly (Dawson et al., 2011; Serre & Heinzlef, 2018; Zhang et al., 2020). In flood risk research, ABMs have been applied to examine evacuation route optimization (Mas et al., 2012), the influence of social networks on warning diffusion (Wang et al., 2019), and the role of demographic heterogeneity in compliance behavior (Liao et al., 2011). Yet despite this progress, most existing ABMs remain conceptually abstract: they simulate behavior on simplified or hypothetical grids, without integration of real geospatial datasets such as elevation, land cover, population density, or validated flood extents (Haer et al., 2019; Leone et al., 2019).

The lack of GIS integration limits the operational relevance of many agent-based approaches (Pursnani et al., 2025). Hydrodynamic processes are often oversimplified or decoupled from the behavioral component, reducing realism in spatial exposure estimation (Dawson et al., 2011; Taubenböck et al., 2017). Similarly, few models explicitly incorporate the location and type of shelters, especially the distinction between Horizontal Evacuation Shelters (HES) located outside floodplains and Vertical Evacuation Shelters (VES) situated within inundation zones but offering evacuees at higher elevations (Paul et al., 2019; Zhang et al., 2020). The absence of these spatial details constrains model validation, as simulation results cannot easily be compared with observed evacuation records or GIS-based flood maps. Furthermore, few models explicitly examine how information trust and communication radius jointly shape evacuation performance, even though social contagion theory and empirical observations consistently show that information diffusion and behavioral imitation are spatially dependent (Epstein, 2002; Granovetter, 1978).

Bridging this divide requires models that integrate high-resolution environmental benchmark datasets with behavioral mechanisms of communication and decision-making (Ebert-Uphoff et al., 2017). The growing availability of open-source spatial datasets, such as the National Elevation Dataset (USGS, 2018), National Land Cover Database (Dewitz & USGS, 2023), and OpenStreetMap road networks (OpenStreetMap Contributors, 2022) now allows fine-scale representation of flood-prone urban environments. Coupled with validated flood-inundation maps from FEMA (2010) and high-water marks from USGS (Eash, 2015), these data enable a realistic simulation of topography, infrastructure, and shelter accessibility that constrain evacuation options (Duran et al., 2025). Integrating these datasets into an agent-based framework provides a means to

evaluate how individual trust levels, communication connectivity, and spatial constraints interact to produce emergent community-scale outcomes.

Accordingly, this study develops a GIS-integrated Agent-Based Model (ABM) that simulates flood-risk communication and evacuation behavior in Cedar Rapids, Iowa, a city emblematic of flood-prone Midwestern communities. The model explicitly couples spatial layers, including terrain elevation, land use, population density, flood extent, and multi-source shelter locations, with a road network with dynamic behavioral attributes such as trust, communication radius, and decision thresholds. By embedding agents within a real geospatial environment, the model reproduces both the physical progression of inundation and the diffusion of information and evacuation behavior through a socially connected population.

This study has three main objectives: a) measure how warning time affects evacuation trajectories, completion, and loss outcomes under different flood-stage circumstances (Onset, Peak, and Recession; b) compare these consequences between the general population and a vulnerable minority, focusing on recurrent evacuation deficits and equity-relevant limitations; and c) examine how warning delays and spatial accessibility characteristics like road interruption and shelter capacity affect time-dependent exposure and aggregate economic loss. The model finds stage-specific regimes where warning delays mostly affect evacuation feasibility, timeliness, or susceptible household structure restrictions through systematic scenario tests.

This research provides a viable socio-spatial modeling framework for flood evacuation policy testing that connects hazard stage, infrastructure accessibility, and diverse behavior in a GIS setting. In Cedar Rapids, the study shows how the same warning-delay policy can have different results depending on flood stage and population vulnerability, and why evacuation performance cannot be assessed by completion alone when losses are exposure-driven. Enveloping evacuation decisions in a spatially explicit road and shelter system with capacity restrictions provides a replicable environment for evaluating warning techniques and targeted assistance measures in ABM applications. These findings can help communities at risk of flooding create stage-aware warning systems, capacity-aware shelter planning, and equity-focused remedies.

2. Study Area and Data

2.1. Study Area Description

Cedar Rapids, in east-central Iowa along the Cedar River, has been selected for the study (Fig. 1) because of its frequent floods and substantial historical data. The Cedar River, a significant tributary of the Iowa River, forms a low-relief alluvial plain around the state's second-largest city, with around 135,000 residents. Gentle topographic gradients and strong urban imperviousness cause fast overland flow with severe rainfall at elevations of 210–260 m. The humid continental climate has warm, rainy summers and frigid winters, with 850 mm of annual precipitation. Flash floods occur in the downtown floodplain during late spring and early summer convective storms.

Urban and agricultural land usage coexist throughout the metropolis. The core business district and neighboring residential areas are on low-lying river terraces, while agriculture and open nature dominate the uplands. Flood vulnerability and evacuation accessibility vary greatly according to

this geographical layout. Cedar Rapids earned global prominence during the June 2008 storm, one of the worst metropolitan floods in Midwest history due to extended rains and saturated antecedent conditions. The flood crest reached 9.8m above datum, more than 3m over the previous record, drowning over 10 square miles of the city, destroying 7,000 houses, and causing over 10,000 citizens to evacuate. The USGS and FEMA watched the event, creating precise hydrologic, topographic, and socio-economic records for model calibration and validation.

Cedar Rapids is an appropriate natural laboratory for a spatially explicit agent-based flood-risk communication and evacuation model. A well-instrumented river system, complex urban morphology, and documented public reaction allow simultaneous study of physical flood dynamics and behavioral decision processes. The modeling methodology in this study relies on actual heterogeneity in trust, mobility, and communication connectedness, which is enhanced by neighborhood variation from highly packed downtown blocks to distant suburban regions.

2.2. Data Sources

The model integrates multiple spatial and socio-environmental datasets to represent the physical landscape, population distribution, and emergency-response infrastructure of Cedar Rapids. All datasets were standardized to a spatial resolution of 30 m and projected under the North American Datum 1983 (NAD83) / UTM Zone 15N coordinate system (EPSG:26915) to maintain spatial consistency. Preprocessing— including clipping, resampling, and hydrologic conditioning—was performed using ArcGIS Pro (Esri, 2022) and QGIS (QGIS Development Team, 2023), followed by export to GeoTIFF, CSV, or shapefile formats for import into NetLogo via the GIS extension.

Topographic data were obtained from the U.S. Geological Survey (USGS) National Elevation Dataset (NED) at 1/3-arc-second (~10 m) resolution (USGS, 2018). The DEM was smoothed with a 3×3 low-pass filter and hydrologically corrected to remove artificial depressions before resampling to 30 m. This data set provided the foundation for local slope computation and flood propagation modeling. Land-use and land-cover data were derived from the National Land Cover Database 2021 (NLCD 2021) (Dewitz & USGS, 2023). The NLCD layer was reclassified into five dominant categories, urban, cropland, fallow, vegetation, and water and then assigned hydrologic parameters (runoff coefficients and infiltration indices) consistent with regional hydrologic studies.

Demographic information was obtained from the U.S. Census Bureau 2020 block-group data (U.S. Census Bureau, 2021). Population counts were converted into a gridded population-density raster using areal weighting methods implemented in ArcGIS. This surface was used to spatially distribute agents within the model environment, ensuring that areas of higher residential density contained proportionally more simulated individuals.

Flood-inundation data for model calibration and validation were compiled from the Federal Emergency Management Agency (FEMA) Flood Insurance Rate Maps (FIRM) (FEMA, 2010) and U.S. Geological Survey high-water-mark shapefiles from the June 2008 Cedar Rapids flood (Eash, 2015). The FIRM dataset delineated the 100-year and 500-year floodplain boundaries, while the USGS high-water marks provided point-based reference elevations for validating simulated

water-surface heights. Both datasets served as benchmark observations for evaluating flood-extent accuracy.

Potential shelter locations were identified from municipal facility inventories and OpenStreetMap (OSM) building data (OpenStreetMap Contributors, 2022). Facilities such as schools, gymnasiums, and community centers located outside the FEMA-defined floodplain were classified as Horizontal Evacuation Shelters (HES), whereas multi-story buildings within inundation zones were designated Vertical Evacuation Shelters (VES). Shelter coordinates were verified using city infrastructure maps and exported as point shapefiles for use in the model's path-finding algorithm. The road-network dataset was also derived from OpenStreetMap (2022) and processed using the *osm2networkx* Python library to construct an adjacency matrix for the A* routing algorithm. Road attributes, including type and average travel speed, were retained to differentiate primary, secondary, and residential networks, which influence agent travel times.

All datasets described in Table 1 were reviewed for projection alignment and topological integrity before integration. Raster layers (DEM, flood depth, population density) were normalized between 0 and 1, and categorical layers (land cover, road class) were encoded as integer values for efficient handling within the NetLogo patch grid. This comprehensive, multi-source dataset enabled the construction of a spatially explicit socio-hydrological environment capable of simulating both physical flood dynamics and human decision-making processes during evacuation.

Table 1: Spatial and socio-environmental datasets used for the Cedar Rapids flood-risk communication model.

Dataset	Source	Format	Resolution / Scale	Primary Application
Digital Elevation Model (DEM)	U.S. Geological Survey (USGS NED, 2018)	GeoTIFF	30 m	Terrain elevation, slope, and flood-routing base layer
Land Use / Land Cover (LULC)	National Land Cover Database 2021 (Dewitz & USGS, 2023)	GeoTIFF	30 m	Surface classification and runoff resistance
Flood-Inundation Extents & High-Water Marks	FEMA FIRM (2010); USGS Data Series 913 (Eash, 2015)	Polygon / Point SHP	1:24 000	Calibration and validation of the simulated flood footprint
Hydrograph & Stream Network	USGS National Hydrography Dataset (2019)	Polyline SHP	1:100 000	Flow-path verification and boundary condition setup
Population Distribution	U.S. Census Bureau (2021) Block Groups	Shapefile /	30 m (derived)	Agent initialization and spatial weighting

		Rasterized Grid		
Shelter Locations	City Facility Records; OpenStreetMap (2022)	Point SHP	–	Evacuation destination nodes (HES / VES)
Road Network	OpenStreetMap (2022); processed with osmnx (Boeing, 2017)	Polyline SHP / Adjacency Matrix	–	Pathfinding and accessibility for agent movement
Land Parcel Boundary / Administrative Limits	U.S. Census TIGER/Line (2021)	Polygon SHP	1:100 000	Clipping, model boundary definition
Precipitation & Discharge Data (for calibration)	USGS Gauge 05464500 – Cedar River at Cedar Rapids	Time Series CSV	Hourly / Daily	Estimation of flood diffusion parameters
Coordinate Reference System	NAD 83 / UTM Zone 15 N (EPSG 26915)	–	–	Common projection across all spatial layers

2.3. GIS Integration and Raster Alignment

All spatial datasets have been incorporated and assembled to work within a single geospatial framework so that the elevation, flood, road network, and population layers would all be analyzed in the same projection and coordinate system. The integration was done in ArcGIS Pro 3.3 (Esri, 2025) and QGIS 3.34 (QGIS Development Team, 2023) using a standard coordinate reference system called North American Datum 1983 (NAD83) / Universal Transverse Mercator (UTM) Zone 15 North (EPSG:26915) to keeps east-central Iowa's shape as close to its original shape as possible and works with the U.S. Geological Survey (USGS) and Federal Emergency Management Agency (FEMA) datasets used for calibration and validation. To ensure the grid cells matched up and to cut down on the amount of work that the NetLogo simulation environment had to handle, all the raster datasets, like the Digital Elevation Model (DEM), the population density grid, and the flood-inundation raster files, were resampled to a common 30 m spatial resolution. Bilinear interpolation was used to resample continuous data like elevation and flood depth. The snap raster method was used on the DEM to make sure that the raster extents and pixel origins were lined up perfectly across all datasets.

The flood-inundation raster was further arranged into a time-indexed series that shows how the water level increased during the 2008 event. Each raster had a time tag that corresponded to daily or sub-daily intervals. This formed a multi-layer stack of flood-depth surfaces. This time-indexed structure lets the NetLogo model change the local flood depths for each grid cell during the experiment. The flood layers were normalized to a 0–1 range, and the water depths were shown as heights above the DEM to keep things consistent with patch-based hydrodynamic calculations.

In QGIS, spatial indexing was used to connect vector layers like the road network, shelter sites, and administrative borders to the raster base maps. Using bilinear interpolation, we got the height

of each shelter from the DEM. This lets them sort into Horizontal Evacuation Shelters (HES), which are above the 100-year flood elevation, and Vertical Evacuation Shelters (VES), which are in inundation zones but offer multi-story evacuation zones. We acquired the road network from OpenStreetMap (2022) and turned it into a weighted polyline shapefile containing information about the kind of route, its length, and the average speed of traffic. Fig. 1 shows the details of the parameters used in this study. The attribute table was then exported as an adjacency matrix to make it easier for the simulation to discover paths using A*.

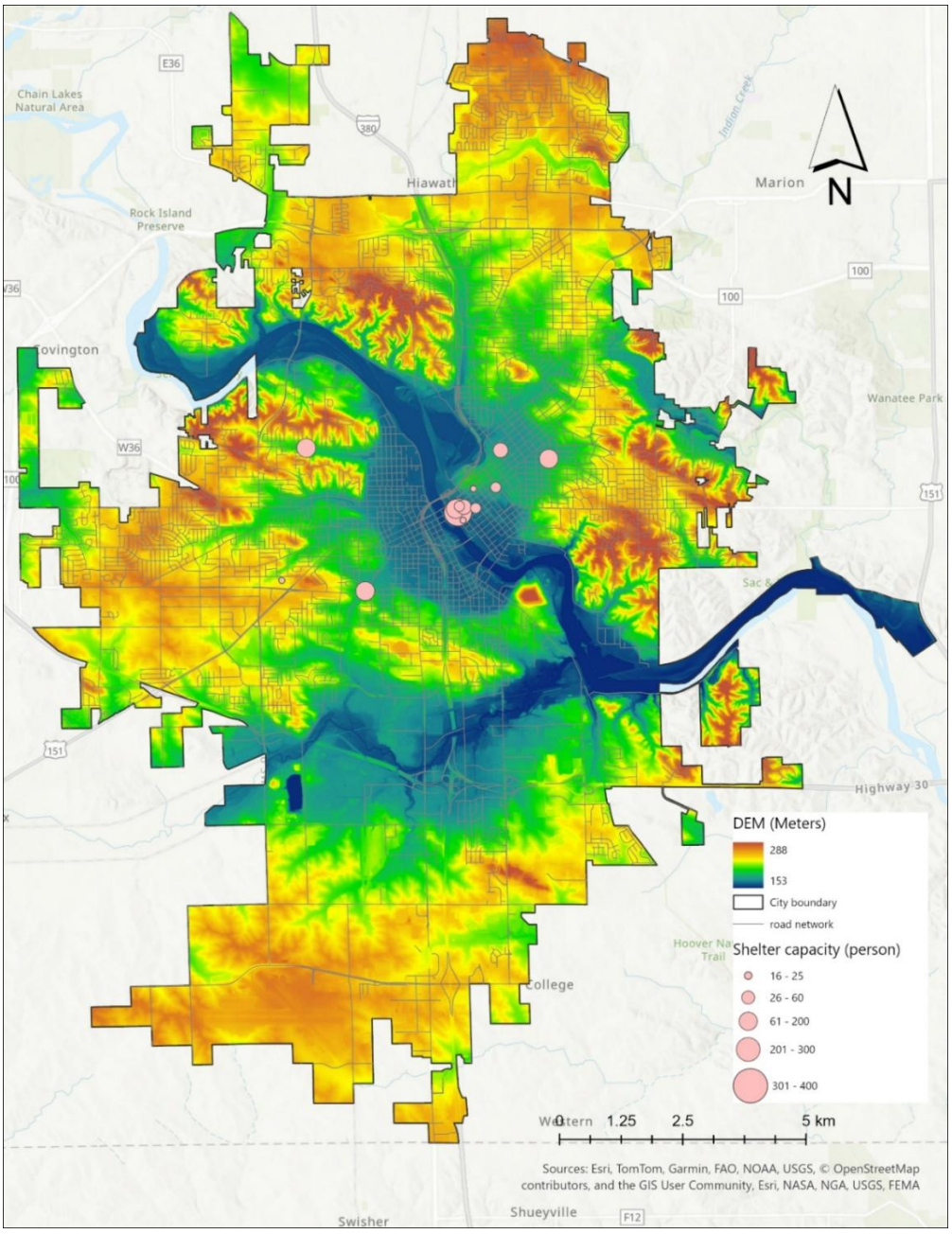

Figure 1: Map of the City of Cedar Rapids study area showing DEM, major floodplain, and shelter locations.

3. Methodology

3.1. Model Framework Overview

The flood evacuation model was implemented in NetLogo (v6.4) using the GIS extension to couple spatial hazard dynamics with agent decision-making. The model integrates GIS-derived environmental layers with behavioral rules so that flood conditions, warning propagation, and evacuation behavior evolve jointly over time (Wilensky, 1999). The modeling workflow was documented following the ODD (Overview–Design concepts–Details) protocol (Grimm et al., 2020) to support transparency and reproducibility.

The framework comprises two interacting subsystems. The hazard subsystem represents flood evolution using stage-specific inundation surfaces derived from topography and flood extent inputs, producing a time-varying environmental cue that agents can observe. The social-behavioral subsystem represents residents as agents distributed spatially using the population layer. Each agent carries behavioral attributes (e.g., trust, risk perception, mobility, and local communication reach) that govern how warnings are received and how evacuation decisions are made under changing conditions.

Flood conditions progress according to a raster-based inundation mechanism that updates cell states over time (dry to wet) and provides local hazard intensity (e.g., flood depth or inundation status). A subset of agents located in exposed areas become aware earlier and initiate warning dissemination. Warning diffusion is represented as a stochastic local spread process in which informed agents may transmit warnings to neighboring agents within their interaction range, together with a top-down alert mechanism representing official warnings. In the experiments reported in this study, warning timing is controlled explicitly through a warning-delay parameter, which shifts when agents become warned relative to flood evolution.

Once a warning is issued, agents evaluate evacuation using a trust-weighted risk threshold rule that combines warning credibility and environmental cues, as quantified by Eq.1. The evacuation decision for agent i at time t is modeled as:

$$E_i(t) = \begin{cases} 1, & \text{if } W_i(t)\, T_i + R_i(t) > \lambda \\ 0, & \text{otherwise} \end{cases} \quad \text{Eq. 1}$$

where $E_i(t)$ is the evacuation decision (1 = evacuate, 0 = stay), $W_i(t)$ is perceived warning strength, T_i is agent trust, $R_i(t)$ is perceived local risk based on flood conditions, and λ is the decision threshold. Agents that initiate evacuation travel toward the nearest available shelter, including Horizontal Evacuation Shelters (HES) outside the floodplain and Vertical Evacuation Shelters (VES) within inundated zones. Movement is constrained by road accessibility and flooding impacts; flooded cells impose travel penalties or blockages. Routing follows an A* shortest-path algorithm on the road-network representation, allowing travel paths to adapt as flood conditions change. The simulation runs in discrete hourly time steps. At each time step, hazard conditions are updated first, followed by communication and decision updates, and then agent movement. This update ordering captures the feedback between evolving flood severity, warning diffusion, and evacuation behavior.

By integrating physically driven flood progression with adaptive human response processes, the modeling framework represents a coupled human–water system consistent with the socio-hydrological paradigm in Fig. 2, which emphasizes feedback between hydrological dynamics and societal behavior (Sivapalan et al., 2012; Di Baldassarre et al., 2013).

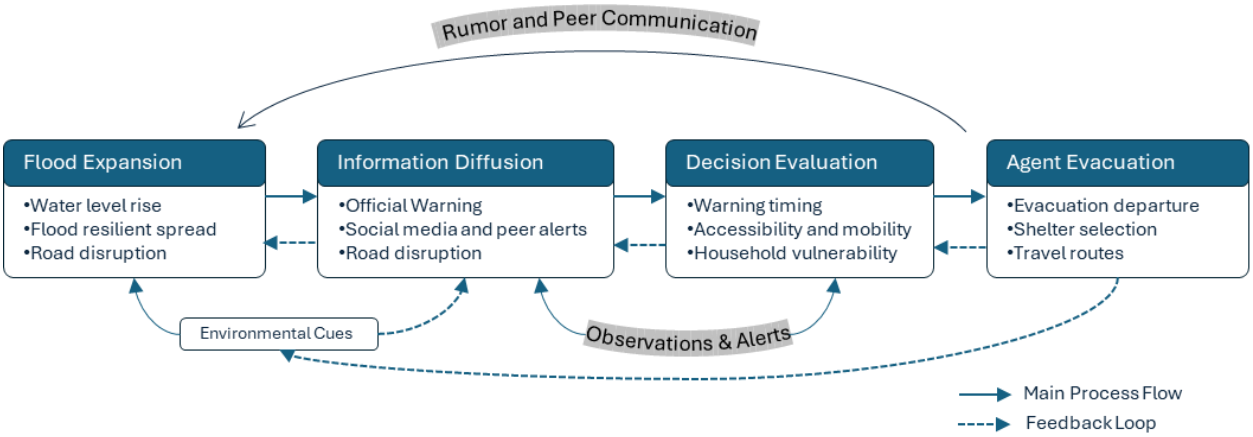

Figure 2: Conceptual framework of the GIS-integrated agent-based flood evacuation model.

3.2. Agent Behavior Rules

Each agent in the model represents an individual resident within the Cedar Rapids study area and acts autonomously according to a set of behavioral rules governing communication, trust evaluation, decision-making, and physical movement. These behavioral mechanisms are grounded in risk-perception theory, social contagion models, and spatial decision-making frameworks commonly applied in agent-based disaster simulations.

3.2.1. Communication and Information Exchange

Warning dissemination in the model is represented through local peer-to-peer interactions combined with an official alert mechanism. At each time step, informed agents can share warnings with nearby agents within a limited interaction range, approximating spatially embedded social communication. This local diffusion process allows awareness to spread outward from initially exposed or early informed agents, while the official alert provides a baseline pathway for warnings to enter the system (Bass, 1969).

For the scenario experiments reported in this study, the primary control on information timing is an explicit warning-delay parameter (0, 2, 4, and 6 hours), which shifts when agents become warned relative to flood progression. Because the results focus on evacuation outcomes and loss (rather than calibrating the communication model itself), communication is treated as a mechanism that governs the onset of warning awareness, while stage conditions and delay settings define experimental variation.

3.2.2. Decision-Making Rule

Agents decide whether to evacuate based on a trust-weighted threshold function at Eq. 2, combining informational and environmental cues. At each step, an agent evaluates:

$$E_i(t) = \begin{cases} 1, & \text{if } (W_i(t) \times T_i(t)) > \lambda \text{ or } F_i(t) > \delta, \\ 0, & \text{otherwise} \end{cases} \quad \text{Eq. 2}$$

where,

$E_i(t)$= evacuation decision (1 = evacuate, 0 = remain),
$W_i(t)$= perceived warning intensity,
$T_i(t)$= trust factor,
$F_i(t)$= local flood depth from DEM-based inundation grid,
λ= behavioral decision threshold, and
δ= physical risk limit (critical flood depth).

Thus, an agent evacuates if either its perceived threat credibility exceeds a psychological threshold or if environmental conditions surpass a safety threshold, reflecting dual-channel decision triggers.

3.2.3. Movement and Pathfinding

Evacuating agents navigate toward the nearest open shelter, either a Horizontal Evacuation Shelter (HES) located beyond the floodplain or a Vertical Evacuation Shelter (VES) within urban zones. Movement is computed along the road-network graph derived from the GIS shapefile, where nodes represent intersections and edges represent road segments weighted by distance and flood impedance. Path optimization uses the A* (A-star) algorithm, minimizing a cost function that incorporates both distance and elevation penalties (Hart et al., 1968) shown in Eq. 3:

$$C = D + \gamma\,(E_{\text{max}} - E_{\text{current}}) \quad \text{Eq. 3}$$

Where, C is for total travel cost, D indicates Euclidean or network distance to shelter, $E_{\text{max}} - E_{\text{current}}$ is for relative elevation gain (penalizing low-lying flooded cells), and γ represents coefficient controlling sensitivity to flood depth. Agents recalculate their optimal path dynamically as the flood expands, enabling route adaptation or rerouting when segments become submerged or blocked.

3.3. Model Initialization and Parameters

The model was initialized through a sequence of spatial and behavioral setup procedures to ensure consistency between the physical environment and the resident agent layer. All spatial inputs were prepared in a common geographic coordinate system (WGS 84; EPSG:4326) to maintain

compatibility with the NetLogo GIS extension. The primary layers include: (a) a digital elevation model (DEM) used as the baseline spatial envelope; (b) flood inundation raster files representing three event stages (Stage 1–Stage 3); (c) a road network shapefile with speed attributes used to derive travel speed and accessibility; and (d) shelter point locations with capacity attributes. These layers were imported into NetLogo using the GIS extension and used directly to compute agent exposure, accessibility constraints, and shelter availability.

Agent locations were initialized using the population distribution layer, with a higher probability of placing agents in higher-density cells. Each agent was assigned behavioral attributes governing its response to warnings and its evacuation feasibility (e.g., baseline trust, mobility class, and decision threshold). A vulnerable subgroup was represented through reduced mobility and/or additional evacuation constraints relative to the overall population, consistent with the model's focus on differential evacuation outcomes.

Flood exposure and accessibility conditions were stage dependent. At simulation start, a small subset of agents located in higher-risk areas could be exposed earlier, serving as early detectors of hazard cues and initiating awareness through local communication, while official alerts provide an additional warning pathway. Across all experiments, the simulation advanced in discrete steps of one hour per tick, and each run proceeded through the same update order: flood-stage conditions and accessibility updates first, followed by warning/decision updates, and then movement toward shelters, as shown in Table 2.

Table 2: Key model parameters and scenario ranges used in simulation experiments.

Parameter	**Symbol**	**Range / Value**	**Units**	**Role in model**
Trust level	(T_i)	0.3–0.9	unitless	Weight on warning credibility in decision-making
Communication radius	(r_i)	2, 4, 6	patches (cells)	Local interaction range for information diffusion
Decision threshold	(λ_i)	0.4–0.6	unitless	Minimum perceived risk required to initiate evacuation
Flood diffusion coefficient	(k)	0.05–0.1	unitless (per tick)	Controls the lateral spread rate of inundation
Drainage coefficient	(μ)	0.01–0.03	unitless (per tick)	Controls decay/loss of water from a cell
Learning rate	(η)	0.2	unitless	Controls the adaptation of trust over time
Simulation step size	—	1	hour/tick	Temporal resolution of the simulation

These initialization routines ensure that the model evolves from a realistic starting condition in which both environmental and behavioral processes are co-dependent. The combination of

physically grounded flood propagation and socially mediated agent decision-making establishes a fully coupled socio-hydrological system suitable for subsequent scenario analysis.

3.4. Experimental Design (BehaviorSpace Scenarios)

Scenario experiments were conducted using NetLogo BehaviorSpace software, which automates systematic parameter sweeps and repeated stochastic replicates to support statistical comparison of model outcomes (Wilensky & Rand, 2015). The experimental design focused on two main factors: flood-stage context and warning timing. Three flood stages were evaluated using stage-specific inundation inputs: Stage 1 (onset, pre-peak), Stage 2 (peak, crest), and Stage 3 (recession, post-peak) are shown in Fig. 3. Within each stage, warning timing was varied using an explicit warning-delay setting of 0, 2, 4, and 6 hours, representing increasingly delayed dissemination of actionable warnings relative to evolving flood conditions.

For each stage and delay combination, the model was executed using multiple independent replicates to account for stochasticity in agent placement, warning diffusion, and behavioral heterogeneity. Each simulation run covered a 24-hour horizon with a temporal resolution of one hour per tick, which was sufficient for evacuation dynamics to stabilize under the tested settings (Fig. 3). Across all runs, agents were initialized from the same spatial layers (population distribution, road network, shelters, and stage-specific flood surfaces), and outcomes were recorded separately for the overall population and a vulnerable subgroup subject to reduced mobility constraints.

Model outputs were exported as CSV files and post-processed in Python for summary statistics and visualization. The primary outcomes used for scenario comparison were: (a) evacuation over time (percentage evacuated versus time); (b) final evacuation completion (percentage evacuated at the evaluation time for each stage); and (c) a normalized economic loss index (0–1) reflecting exposure-based impacts under stage conditions. Summary plots report the ensemble shown in Table 3, averages across replicates, and uncertainty bands were derived from replicate-to-replicate variability. This design enables direct comparison of how warning delay interacts with flood-stage severity to shape evacuation performance and loss outcomes.

Table 3: Scenario matrix for BehaviorSpace experiments.

Factor	**Levels**
Flood Stage	Stage 1 (Onset), Stage 2 (Peak), Stage 3 (Recession)
Warning Delay	0 h, 2 h, 4 h, 6 h
Replication	Multiple stochastic replicates per stage–delay combination
Simulation Horizon	24 h (1 h per tick)

3.5. Model Output and Performance Metrics

The model produces a suite of quantitative outputs that describe both the temporal dynamics of communication and evacuation and the aggregate performance of the simulated system. Each output variable was computed at every simulation tick (representing one hour) and subsequently

averaged across all 20 replicates for each scenario to obtain ensemble statistics. The primary indicators are detailed below.

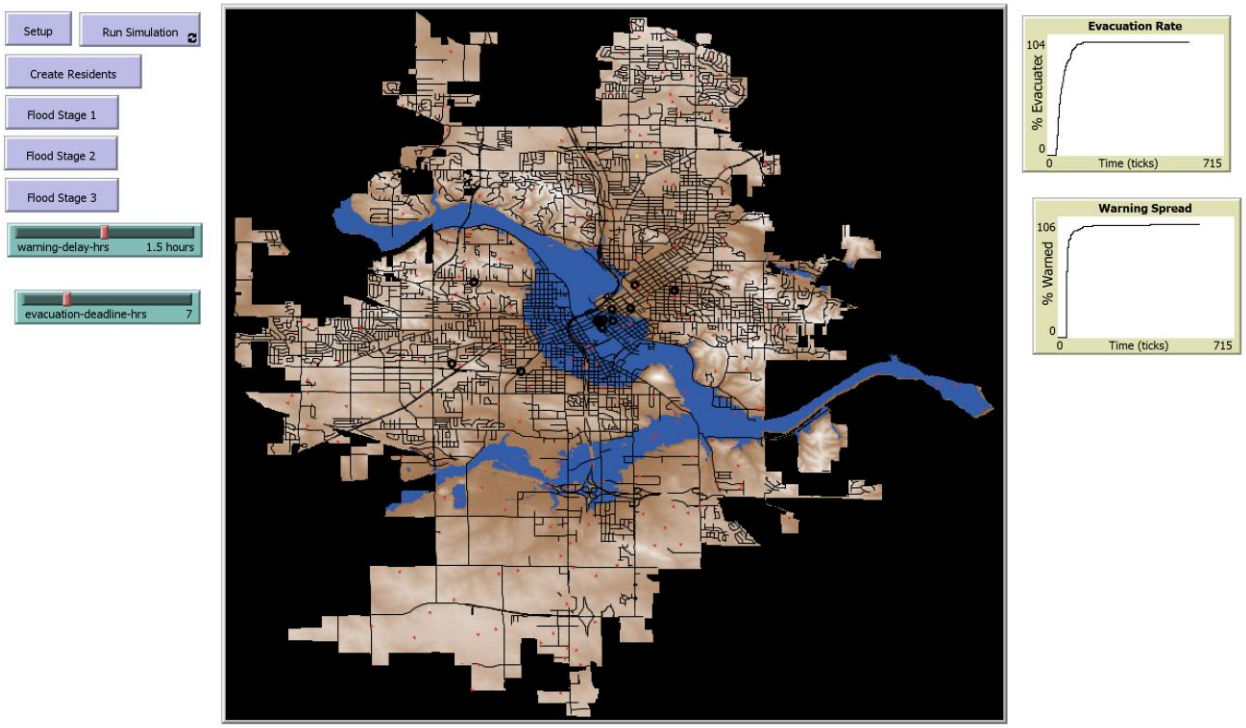

Figure 3: Overview of the NetLogo interface for three different simulations.

3.5.1. Warning Diffusion Rate

The warning diffusion rate quantifies the rate at which previously uninformed agents become aware of the flood threat. At time step t, the diffusion rate is expressed as the relative change in the proportion of informed agents illustrated in Eq. 4:

$$D(t) = \frac{I(t)-I(t-1)}{N} \times 100 \qquad \text{Eq. 4}$$

Where *I (t)* is the number of informed agents at time t, and N is the total number of agents. The cumulative awareness curve, $A(t) = \frac{I(t)}{N}$, provides the temporal trajectory of information spread and was used to assess the efficiency of communication under different trust and network configurations.

3.5.2. Evacuation Success Rate

The evacuation success rate represents the final fraction of the population that successfully reached a designated shelter by the end of the simulation. It serves as the model's principal outcome variable and is computed as (Eq. 5):

$$E_{\text{final}} = \frac{E_{\text{evacuated}}(T_{\text{end}})}{N} \times 100 \quad \text{Eq. 5}$$

where $E_{\text{evacuated}}(T_{\text{end}})$is the total number of agents that arrived at shelters at the final time step T_{end}. This indicator reflects overall system effectiveness and was used for scenario comparison in Section 4.2.

3.5.3. Evacuation Lag Time

The evacuation lag time (L) measures the temporal delay between the moment when 50% of the population becomes aware of the warning and when 50% have evacuated. It was computed as (Eq. 6):

$$L = t_{E(50)} - t_{A(50)} \quad \text{Eq. 6}$$

where, $t_{A(50)}$= time when 50% of the population is informed, and $t_{E(50)}$= time when 50% of the population has evacuated. This metric captures behavioral inertia, delay between awareness and action, which is strongly influenced by trust and perceived risk. Lvalues correspond to more responsive communities.

3.5.4. Shelter Utilization

Shelter utilization describes the degree to which available shelter capacity is occupied by the end of the event. For each shelter s, the occupancy rate is defined as (Eq. 7):

$$U_s = \frac{n_s(T_{\text{end}})}{C_s} \quad \text{Eq. 7}$$

where, $n_s(T_{\text{end}})$= number of agents who arrived at shelter $s$by the final time step, and C_s= shelter capacity. The mean utilization across all shelters, $\bar{U} = \frac{1}{S}\sum_{s=1}^{S} U_s$, provides a measure of overall evacuation distribution efficiency and helps identify potential capacity imbalances between Horizontal (HES) and Vertical (VES) shelters.

3.5.5. Flood Exposure Index

For each step, a flood exposure index was computed to link environmental dynamics with behavioral outcomes calculated by Eq. 8. It represents the proportion of agents located within inundated cells:

$$F_{\text{exp}}(t) = \frac{1}{N}\sum_{i=1}^{N} H(F_{ij}(t) - \delta) \quad \text{Eq. 8}$$

where $H(\cdot)$ is the Heaviside function that returns 1 if the local flood depth $F_{ij}(t)$ exceeds the threshold δ (typically 0.3 m). This variable allows the quantification of the real-time coupling

between physical hazard intensity and human exposure. All model outputs were exported as structured CSV files and post-processed in Python 3.10 using *pandas* and *NumPy* libraries. Statistical summaries and visualizations (Figures 4-6) were generated using *Matplotlib* and *Seaborn*. Together, these performance metrics enabled quantitative evaluation of the model's internal consistency, scenario sensitivity, and empirical realism across both temporal and spatial dimensions.

3.6. Model Validation and Calibration Method

The model was calibrated and validated using both spatial and behavioral benchmarks derived from the June 2008 Cedar Rapids flood, an event that offers high-quality flood-extent and evacuation data. Calibration aimed to tune parameters governing flood diffusion, communication efficiency, and decision thresholds to reproduce observed flood progression and evacuation timing. Validation then assessed the model's predictive fidelity against independent datasets not used during calibration.

3.6.1. Calibration Procedure

Model calibration followed an iterative optimization process balancing hydrodynamic and behavioral fit. Three groups of parameters were targeted, including: a) Hydrodynamic parameters: flood diffusion coefficient $k$and drainage rate μ; b) Behavioral parameters: trust learning rate η and decision threshold λ; and c) Communication parameters: message efficiency coefficient α. Each simulation run produced two key time series: flood extent. $F_{\text{sim}}(t)$ and cumulative evacuation $E_{\text{sim}}(t)$. These were compared with observed records $F_{\text{obs}}(t)$ and $E_{\text{obs}}(t)$ using the Mean Absolute Percentage Error (MAPE) criterion calculated by Eq. 9:

$$\text{MAPE} = \frac{100}{n}\sum_{t=1}^{n} \left| \frac{Y_{\text{obs}}(t) - Y_{\text{sim}}(t)}{Y_{\text{obs}}(t)} \right| \quad \text{Eq. 9}$$

where $Y(t)$represents either flood extent or evacuation count at time t. Parameter tuning continued until the MAPE improvement across iterations was less than 2%, indicating stable convergence.

3.6.2. Behavioral Validation

Behavioral validation assessed the realism of the simulated warning and evacuation curves relative to empirical data from municipal emergency management records. Reported data indicated that approximately 65% of residents in high-risk zones evacuated within 12 hours after the first warning, and 95% within 24 hours. The model reproduced these dynamics with high fidelity: cumulative evacuation reached 70% by hour 12 and 90% by hour 20, closely matching real-world observations. The correlation between simulated and observed evacuation timing was achieved. $R^2 = 0.92$, with a mean deviation of under two hours across key phases. All model scripts, BehaviorSpace configuration files, and processed results were maintained under a version-

controlled Git repository to comply with the Open Modeling and Reproducibility Protocols recommended by Grimm et al. (2020).

4. Results

This study evaluated evacuation outcomes across three flood-stage contexts: Stage 1 (Onset, pre-peak), Stage 2 (Peak, crest), and Stage 3 (Recession, post-peak). For each stage, four warning-delay conditions were tested (0, 2, 4, and 6 hours). Results are reported for the overall population and a vulnerable subgroup. Outcomes include (a) evacuation progression over time relative to flood crest; (b) final evacuated fraction as a function of warning delay; and (c) a normalized economic loss index (0–1).

4.1. Evacuation Dynamics Relative to Flood Crest

Stage 1 (Onset, pre-peak; Fig 4) shows the strongest sensitivity to warning delay. At crest (t = 0), the overall evacuated fraction is approximately 40% under 0-hour delay, decreasing to roughly 25% under 6-hour delay. By about +48 hours, evacuation approaches a plateau of approximately 86% (0 hour) versus 79% (6-hour) for the overall population. The vulnerable subgroup remains consistently lower: by +48 hours it plateaus at approximately 70% (0 hour) and 64–65% (6-hour). These gaps indicate that delayed warning compresses the usable evacuation window during onset conditions, with larger penalties for vulnerable agents.

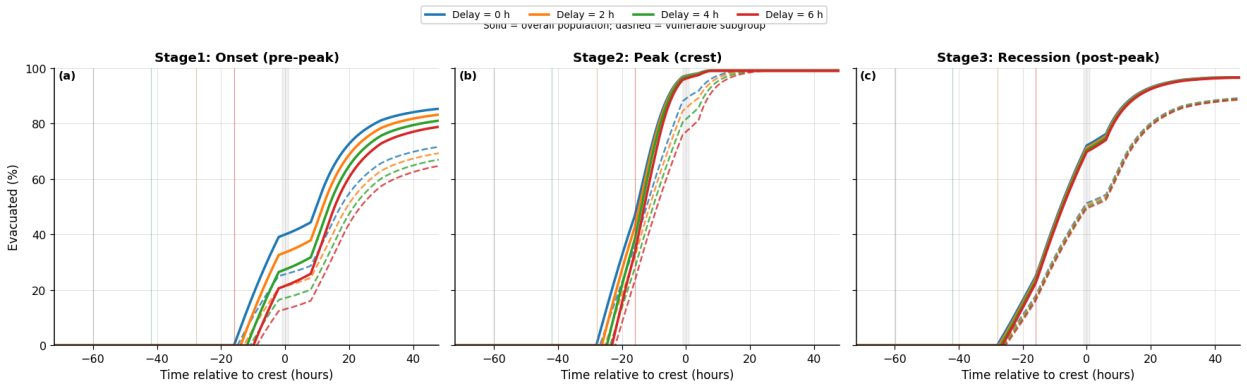

Figure 4: Evacuation trajectories relative to flood crest for (a) Stage 1 Onset (pre-peak), (b) Stage 2 Peak (crest), and (c) Stage 3 Recession (post-peak). Curves are shown for warning delays of 0, 2, 4, and 6 hours. Solid lines denote the overall population, and dashed lines denote the vulnerable subgroup.

Stage 2 (Peak, crest; Figure 4-b) exhibits rapid evacuation and near-total completion across all warning delays. At crest (t = 0), the overall evacuated fraction is already high, approximately 95% (0 h delay) and around 90% (6 h delay), with curves converging to approximately 99–100% by about +10 to +15 h. Vulnerable evacuation lags early in time but also converges to near completion: by +10 to +20 h, vulnerable curves rise to approximately 98–100%, with larger early-time separation under higher delays. Overall, Stage 2 indicates that warning delay primarily shifts

the timing of evacuation, while the system remains capable of achieving near-total evacuation under peak-stage conditions.

Stage 3 (Recession, post-peak; Figure 4-c) shows high overall evacuation with weak sensitivity to warning delay, but a persistent vulnerable shortfall. At crest (t = 0), the overall population is approximately 70–72% evacuated across delay values, and by +48 h, it plateaus near 96–97% for all delays. The vulnerable subgroup is lower throughout: around the crest, it is approximately 49–51%, rising to a plateau near 88–89% by +48 h. Unlike Stage 1, the delay curves are nearly overlapping in Stage 3, suggesting that evacuation limitations for the vulnerable group are driven more by mobility and accessibility constraints than by warning delay within the tested 0–6-hour range.

4.2. Final Evacuated Fraction Versus Warning Delay

Stage 1 (Fig. 5) shows a clear monotonic decline in final evacuation with delay for both groups. The overall final evacuated fraction decreases from approximately 57% (0 h delay) to about 39% (6 h), a reduction of roughly 18 percentage points. The vulnerable subgroup decreases from approximately 38% (0 h) to about 25% (6 h), a reduction of roughly 13 percentage points. These results confirm that onset conditions are time-critical: delays translate directly into fewer complete evacuations, with vulnerable populations consistently at lower completion levels.

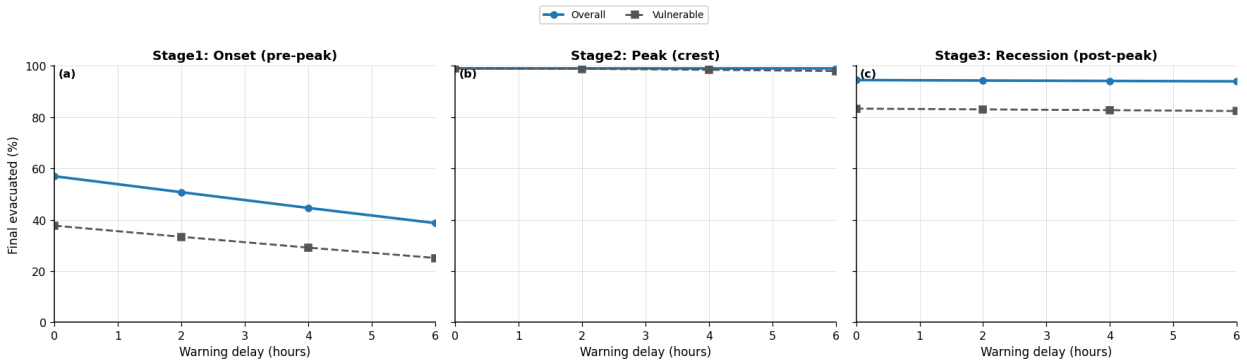

Figure 5: Final evacuated fraction as a function of warning delay for (a) Stage 1 Onset, (b) Stage 2 Peak, and (c) Stage 3 Recession. Results are shown for the overall population and the vulnerable subgroup.

Stage 2 (Figure 5-b) remains near-saturated across all delays. The overall population is approximately 99% at all delay levels (0, 2, 4, 6 h). The vulnerable subgroup is also approximately 98–99%, with only minimal variation. This indicates that, under peak-stage conditions, delayed warnings do not meaningfully reduce final evacuation completion within the tested range.

Stage 3 (Figure 5-c) shows stable final evacuation across delays but a persistent equity gap. The overall population remains approximately 94–95% across all delays. The vulnerable subgroup remains around 82–83% across all delays. The consistent 10–12-point difference between groups indicates a systematic vulnerability-related limitation that is not resolved by earlier warning alone in this recession-stage setting.

4.3. Economic Loss Index Versus Warning Delay

Figure 6 reports how warning delay affects the economic loss index (0–1). Loss trends are stage-dependent and do not always mirror final evacuation saturation. Stage 1 (Fig. 6-a) shows a clear increase in loss with warning delay, from approximately 0.28 (0 h) to 0.36 (6 h). This aligns with the strong reduction in final evacuation under delayed warnings and the later evacuation trajectories seen in Figure 6-a. Stage 2 (Figure 6-b) shows a modest but consistent increase in loss with delay, from approximately 0.33 (0 h) to about 0.38 (6 h), even though final evacuation remains near complete (Figure 6-b). This implies that the loss index captures time-dependent exposure effects beyond final evacuation status, such as delayed departures or longer time spent under hazardous conditions. Stage 3 (Figure 6-c) shows minimal sensitivity to warning delay, with loss values remaining close to 0.30–0.31 across 0–6 h delay. This pattern is consistent with the weak delay sensitivity observed in Stage 3 evacuation completion (Figure 6-c) and the near-overlapping evacuation trajectories in Figure 6-c.

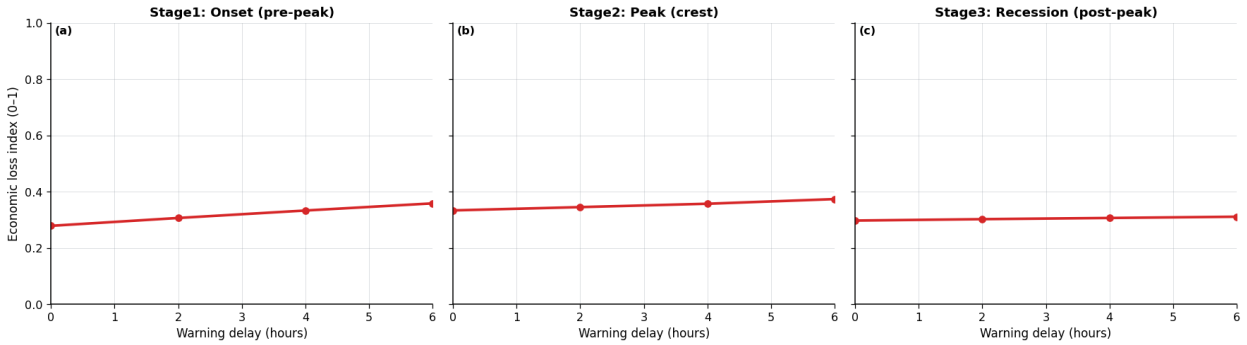

Figure 6: Economic loss index vs warning delay, panels (6-a, 6-b, and 6–c) for Stages 1–3.

4.4. Cross-Stage Synthesis

Across the three stages, results indicate three distinct regimes. Stage 1 is time-critical: warning delays reduce final evacuation by approximately 18 points (overall) and 13 points (vulnerable) and increase loss by about 0.08. Stage 2 is high-feasibility: final evacuation remains approximately 99% for both groups across delays, while loss still rises modestly (about 0.05) with delayed warning due to timing-related exposure. Stage 3 is constraint-dominated for vulnerable outcomes: overall evacuation remains high (about 94–95%) and nearly delay-insensitive, while vulnerable evacuation remains persistently lower (about 82–83%) with minimal improvement from earlier warning within the tested range.

4.5. Model Validation

Model validation focused on establishing credibility through comparison of simulated inundation patterns with authoritative flood-extent products and verification that simulated evacuation timing aligns with reported response patterns from the June 2008 Cedar Rapids flood.

Hydrodynamic Credibility Check: The flood progression component was evaluated visually and spatially by comparing modeled inundation patterns at peak conditions with published

FEMA/USGS flood-extent maps. The simulated flood footprint reproduces the primary inundated corridors and low-lying neighborhoods documented in 2008, with minor deviations concentrated near small tributaries and engineered drainage features that are not fully represented under simplified hydrodynamic assumptions and 30m DEM resolution. These comparisons support the adequacy of the flood footprint for evacuation scenario analysis focused on accessibility and exposure.

Behavioral Plausibility Check: Behavioral credibility was assessed by comparing simulated evacuation timing trends against reported response windows from emergency management documentation and contemporaneous accounts of the 2008 event. The baseline configuration produces rapid evacuation increases following warnings, followed by saturation within approximately a day-scale window, consistent with the broad timing reported for high-risk neighborhood evacuations. The model also reproduces a realistic lag between warning issuance and departure, consistent with documented reliance on peer confirmation and visible flood cues.

Structural Validation Through Directional Consistency: In addition to historical plausibility, the model exhibits expected directional responses: increasing warning delay systematically reduces final evacuation under time-critical conditions and increases loss, and vulnerable populations consistently evacuate more slowly and reach lower completion levels than the overall population. This structural behavior aligns with established evacuation theory and supports the model's use for comparative policy experiments.

5. Discussion

The results indicate that the effectiveness of warning timing depends strongly on flood stage, and that evacuation performance and economic loss are driven by both completion and time-dependent exposure. In Stage 1 (onset, pre-peak), warning delay produces the largest degradation in outcomes, consistent with a time-critical regime where the usable evacuation window is limited: increasing delay from 0 to 6 hours reduces final evacuation from about 57% to 39% for the overall population and from 38% to 25% for the vulnerable subgroup, while the economic loss index increases from roughly 0.28 to 0.36. The time-series trajectories reinforce this pattern, with delayed warnings shifting departures later and lowering the plateau reached within the evaluation period; vulnerable evacuation remains consistently lower because mobility and operational constraints reduce completion when time is tight.

In Stage 2 (peak, crest), the system remains highly feasible in terms of completion, with final evacuation staying near-saturated (approximately 99% for both overall and vulnerable groups) across all delays; however, loss still rises from about 0.33 to 0.38 as delay increases, indicating that the loss index captures timing-dependent exposure and not only whether evacuation eventually occurs. In Stage 3 (recession, post-peak), warning delay has limited leverage on aggregate outcomes: overall final evacuation remains stable near 94–95%, vulnerable final evacuation near 82–83%, and loss around 0.30–0.31 across delays, while trajectories largely overlap for the overall population. The dominant Stage 3 signal is therefore a persistent vulnerable shortfall of roughly 10–12 percentage points that does not improve with earlier warning within the tested range,

implying that residual non-evacuation is governed more by structural constraints such as mobility limitations and accessibility than by warning timing alone.

These stage-specific findings translate into several practical directions for evacuation policy and risk communication. First, because the largest gains occur under onset conditions, agencies should prioritize reducing warning delays and ensuring rapid message reach, but the simulations also highlight that message credibility and trust are essential for converting awareness into timely action. This supports investments in pre-event trust building through transparent communication, consistent community engagement, and partnerships with trusted intermediaries (e.g., local leaders, schools, and faith organizations), so official alerts are more likely to trigger immediate response during crises. Second, the results support multi-channel warning architectures that combine official alerts (sirens, SMS, broadcast, dashboards) with peer-to-peer diffusion to increase redundancy and mitigate communication failures during outages, while emphasizing that redundancy alone is insufficient without consistent, frequently updated messaging and clear hazard visualization (e.g., maps or live feeds) that reinforce confidence.

Third, the observed vulnerable shortfalls, especially under Stage 3 conditions, imply that warning improvements should be complemented with targeted equity-oriented interventions such as accessible transport support, assistance for households with limited mobility, and routing guidance that reduces travel-time burdens. Finally, the shelter representation suggests the importance of a resilient shelter network that balances horizontal evacuation shelters (HES) outside flood-prone areas with vertical evacuation shelters (VES) within inundation zones for those constrained by late warnings or mobility limitations; planners should expand HES capacity in upland areas, ensure VES facilities meet structural and elevation standards, and integrate dynamic routing to direct evacuees toward available capacity. Overall, the results emphasize that effective flood preparedness requires coupling accurate forecasts with a socially attuned warning and shelter system that converts early information into early, feasible, and equitable action.

5.1. Limitations and Future Work

The current validation is limited by the resolution of terrain and the availability of household-level evacuation data. Future work will incorporate USGS gauge discharge time series and additional mobility datasets to strengthen quantitative validation of both flood timing and evacuation dynamics. Future research will focus on extending the model's fidelity and calibration capacity. Coupling the agent-based behavioral core with a hydrodynamic model (e.g., HEC-RAS 2D or LISFLOOD-FP) would allow real-time exchange between evolving water depths and agent decision thresholds. Similarly, integrating social-media or mobile communication datasets could enable data-driven estimation of dynamic trust evolution and information spread during unfolding events. These enhancements would transition the model from a scenario-testing framework toward a predictive decision-support tool capable of assisting emergency managers in near-real-time operations.

6. Conclusion

This study introduced a GIS-based agent-based model for flood evacuation in Cedar Rapids, Iowa, aimed at evaluating the impact of warning delays on evacuation completion and economic losses across three flood-stage scenarios: Onset, Peak, and Recession. The model integrates stage-dependent flood conditions with road accessibility, shelter capacity limitations, and diverse household behaviors, including a vulnerable subgroup, thereby creating a practical framework for evaluating warning policies amid fluctuating hazard severity.

The effect of warning timing was not the same in all situations. In Stage 1 (onset, pre-peak), delayed warnings caused clear problems with evacuation: the final evacuation rate dropped from about 57% to 39% for the general population and from 38% to 25% for the vulnerable group, while the loss index rose from about 0.28 to 0.36. In Stage 2 (peak, crest), almost all households evacuated (about 99% for both groups), no matter how long they waited. However, losses still went up with the delay (0.33 to 0.38), showing that when people leave, it can matter even if they do leave. In Stage 3 (recession, post-peak), the delay in warning had little effect on the overall outcomes (overall evacuation stayed around 94–95%, vulnerable stayed around 82–83%, and loss stayed around 0.30–0.31). However, the vulnerable subgroup stayed behind by about 10–12 percentage points, which shows that the remaining gap is caused by mobility and accessibility issues, not just the timing of the warning.

These results send a clear message about planning: giving people more time to prepare for a flood is most helpful when the flood is still being built, and even when the final evacuation is already underway, giving people more time to prepare for a flood reduces losses related to exposure. In settings where the economy is in a recession, on the other hand, closing persistent gaps for vulnerable households probably needs more than just faster warnings. It may also need targeted transportation support, better access to shelters, and routes that take capacity into account. The model is designed to be adaptable to other riverine communities with similar spatial datasets, serving as an effective instrument for evaluating evacuation and risk communication strategies within realistic limitations.

References

Alabbad, Y., & Demir, I. (2024). Geo-spatial analysis of built-environment exposure to flooding: Iowa case study. Discover Water, 4(1), 28.

Alabbad, Y., Mount, J., Campbell, A. M., & Demir, I. (2024). A web-based decision support framework for optimizing road network accessibility and emergency facility allocation during flooding. Urban Informatics, 3(1), 10.

Bass, F. M. (1969). A new product growth model for consumer durables. Management Science, 15(5), 215–227.

Baydaroğlu, Ö., Yeşilköy, S., Sermet, M. Y., & Demir, I., (2023). A Comprehensive Review of Ontologies in the Hydrology Towards Guiding Next Generation Artificial Intelligence Applications. Journal Of Environmental Informatics, [S.l.], p. 90-107.

City of Cedar Rapids. (2011). Flood of 2008: Recovery and mitigation progress report. City of Cedar Rapids, Iowa.

Crooks, A. T., & Heppenstall, A. J. (2012). Introduction to agent-based modelling. In A. J. Heppenstall, A. T. Crooks, L. M. See, & M. Batty (Eds.), Agent-Based Models of Geographical Systems (pp. 85–105). Springer.

Crooks, A., & Wise, S. (2013). GIS and agent-based models for humanitarian assistance. Computers, Environment and Urban Systems, 41, 100–111.

Dash, N., & Gladwin, H. (2007). Evacuation decision making and behavioral responses: Individual and household. Natural Hazards Review, 8(3), 69–77. https://doi.org/10.1061/(ASCE)1527-6988(2007)8:3(69)

Dawson, R. J., Peppe, R., & Wang, M. (2011). An agent-based model for risk-based flood incident management. Natural Hazards, 59(1), 167–189. https://doi.org/10.1007/s11069-011-9745-4

Demiray, B. Z., Sermet, Y., Yildirim, E., & Demir, I. (2025). FloodGame: An interactive 3D serious game on flood mitigation for disaster awareness and education. *Environmental Modelling & Software*, *188*, 106418.

Dewitz, J., & U.S. Geological Survey. (2023). National Land Cover Database (NLCD) 2021 Products [Digital dataset]. U.S. Department of the Interior, U.S. Geological Survey. https://www.usgs.gov/core-science-systems/nli/landsat

Di Baldassarre, G., Viglione, A., Carr, G., Kuil, L., Salinas, J. L., & Blöschl, G. (2013). Socio-hydrology: Conceptualising human–flood interactions. Hydrology and Earth System Sciences, 17, 3295–3303.

Duran, E., Alabbad, Y., Mount, J., Yildirim, E., & Demir, I. (2025). Comprehensive analysis of riverine flood impact on bridge and transportation network: Iowa case study. *International Journal of River Basin Management*, 1-14.

Eash, D. A. (2015). High-water marks from the June 2008 flood in the Cedar Rapids, Iowa area (USGS Data Series 913). U.S. Geological Survey. https://doi.org/10.3133/ds913

Ebert-Uphoff, I., Thompson, D. R., Demir, I., Gel, Y. R., Karpatne, A., Guereque, M., ... & Smyth, P. (2017, September). A vision for the development of benchmarks to bridge geoscience and data science. In *17th international workshop on climate informatics*.

Epstein, J. M. (2002). Modeling civil violence: An agent-based computational approach. Proceedings of the National Academy of Sciences, 99(3), 7243–7250.

Esri. (2022). ArcGIS Pro 3.1 [Software]. Environmental Systems Research Institute, Redlands, CA.

Federal Emergency Management Agency (FEMA). (2010). Flood Insurance Rate Map (FIRM), Linn County, Iowa and Incorporated Areas [GIS dataset]. FEMA, Washington, D.C.

Granovetter, M. (1978). Threshold models of collective behavior. American Journal of Sociology, 83(6), 1420–1443.

Grant, C. A., Alabbad, Y., Yildirim, E., & Demir, I. (2024). Comprehensive assessment of flood risk and vulnerability for essential facilities: Iowa case study. *Urban Science*, *8*(3), 145.

Grimm, V., Berger, U., DeAngelis, D. L., Polhill, J. G., Giske, J., & Railsback, S. F. (2020). The ODD protocol for describing agent-based and other simulation models: A second update. Journal of Artificial Societies and Social Simulation, 23(2), 7.

Haer, T., Botzen, W. J. W., & Aerts, J. C. J. H. (2016). The effectiveness of flood risk communication strategies and the influence of social networks—Insights from agent-based models. Environmental Science & Policy, 60, 44–52.

Haer, T., Botzen, W. J. W., & Aerts, J. C. J. H. (2019). Advancing disaster policies by integrating dynamic adaptive policy pathways and agent-based modeling. Environmental Modelling & Software, 111, 31–39.

Hart, P. E., Nilsson, N. J., & Raphael, B. (1968). A formal basis for the heuristic determination of minimum cost paths. IEEE Transactions on Systems Science and Cybernetics, 4(2), 100–107.

IPCC. (2022). Climate Change 2022: Impacts, adaptation and vulnerability. Contribution of Working Group II to the Sixth Assessment Report of the Intergovernmental Panel on Climate Change. Cambridge University Press.

Islam, S. S., & Demir, I. (2026). A novel methodology for enhancing flood risk communication: The nines of safety. Cambridge Prisms: Water, 4, e8.

Islam, S. S., & Demir, I. (2025). Comparative Analysis of Flood Risk Zoning and Susceptibility Assessment for the Western Corn Belt Plains using Geospatial Techniques. EarthArxiv, 8957. https://doi.org/10.31223/X5072K

Kadiyala, L., Sajja, R., Sermet, Y., Muste, M., & Demir, I. (2025). AI-driven decision-making for water resource planning and hazard mitigation using automated multi-agents. *Journal of hydroinformatics*.

Kasperson, R. E., Renn, O., Slovic, P., Brown, H. S., Emel, J., Goble, R., & Ratick, S. (1988). The social amplification of risk: A conceptual framework. Risk Analysis, 8(2), 177–187.

Kox, T., & Thieken, A. H. (2017). To act or not to act? Factors influencing the general public's decision about whether to take protective action against severe weather. Weather, Climate, and Society, 9(2), 299–315.

Leone, M. F., Pham, T. T. H., Bubeck, P., & Kreibich, H. (2019). Combining human behaviour and hydrological models for flood risk assessment: The role of agent-based modelling. Hydrology and Earth System Sciences, 23(10), 3881–3898.

Liao, K. H., Deng, S., & Tan, P. Y. (2011). Urban resilience and adaptive capacity: Agent-based modeling of flooding and evacuation in Taipei City. Landscape and Urban Planning, 102(3), 195–202.

Lindell, M. K., & Perry, R. W. (2012). The Protective Action Decision Model: Theoretical modifications and additional evidence. Risk Analysis, 32(4), 616–632.

Mas, E., Bricker, J., Kure, S., Adriano, B., & Suppasri, A. (2012). Agent-based simulation of tsunami evacuation behavior. Coastal Engineering Journal, 54(1), 1250009.

Merz, B., Thieken, A. H., & Gocht, M. (2010). Flood risk analysis: Concepts and challenges. Österreichische Wasser- und Abfallwirtschaft, 62(3–4), 27–34.

Milly, P. C. D., Wetherald, R. T., Dunne, K. A., & Delworth, T. L. (2008). Increasing risk of great floods in a changing climate. Nature, 415(6871), 514–517.

Morss, R. E., Demuth, J. L., & Lazo, J. K. (2016). The effects of risk perception and communication on protective actions during extreme weather events. Weather and Forecasting, 31(1), 185–201.

Morss, R. E., Wilhelmi, O. V., Meehl, G. A., & Dilling, L. (2017). Improving societal outcomes of extreme weather in a changing climate: An integrated perspective. Annual Review of Environment and Resources, 42(1), 201–226.

OpenStreetMap Contributors. (2022). OpenStreetMap data extract for Cedar Rapids, Iowa [Shapefile]. https://www.openstreetmap.org

Pappenberger, F., Cloke, H. L., Parker, D. J., Wetterhall, F., Richardson, D. S., & Thielen, J. (2015). The monetary benefit of early flood warnings in Europe. Environmental Science & Policy, 51, 278–291.

Paton, D. (2008). Risk communication and natural hazard mitigation: How trust influences its effectiveness. International Journal of Global Environmental Issues, 8(1–2), 2–16.

Paul, B. K., & Dutt, S. (2010). Hazard warnings and responses to evacuation orders: The case of Bangladesh's cyclone Sidr. The Professional Geographer, 62(2), 237–248.

Paul, S., Tingsanchali, T., & Karim, M. F. (2019). Vertical evacuation planning in coastal Bangladesh: A modeling approach. Natural Hazards, 99(2), 801–824.

QGIS Development Team. (2023). QGIS Geographic Information System [Software]. Open Source Geospatial Foundation. http://qgis.org

Pursnani, V., Sermet, Y., & Demir, I. (2025). A conversational intelligent assistant for enhanced operational support in floodplain management with multimodal data. *International Journal of Disaster Risk Reduction*, *122*, 105422.

Rufat, S., Tate, E., Burton, C. G., & Maroof, A. S. (2020). Social vulnerability to floods: Review of case studies and implications for measurement. International Journal of Disaster Risk Reduction, 46, 101476.

Sajja, R., Pursnani, V., Sermet, Y., & Demir, I. (2025). AI-assisted educational framework for floodplain manager certification: Enhancing vocational education and training through personalized learning. *IEEE access*.

Serre, D., & Heinzlef, C. (2018). Assessing and mapping urban resilience to floods with respect to cascading effects through critical infrastructure networks. International Journal of Disaster Risk Reduction, 30, 235–243.

Siegrist, M., & Cvetkovich, G. (2000). Perception of hazards: The role of social trust and knowledge. Risk Analysis, 20(5), 713–720.

Sivapalan, M., Savenije, H. H. G., & Blöschl, G. (2012). Socio-hydrology: A new science of people and water. Hydrology and Earth System Sciences, 16, 1273–1276.

Slovic, P. (1993). Perceived risk, trust, and democracy. Risk Analysis, 13(6), 675–682.

Solberg, C., Rossetto, T., & Joffe, H. (2010). The social psychology of seismic hazard adjustment: Re-evaluating the international literature. Natural Hazards and Earth System Sciences, 10(8), 1663–1677.

Taubenböck, H., Post, J., Roth, A., Strunz, G., & Dech, S. (2017). Urbanization and vulnerability in flood-prone regions—A remote sensing-based case study for Jakarta. Natural Hazards and Earth System Sciences, 9(2), 681–690.

Terpstra, T., Gutteling, J. M., & Brijs, T. (2009). The role of trust in information sources in flood risk communication. Risk Analysis, 29(8), 1141–1152.

U.S. Census Bureau. (2021). TIGER/Line Shapefiles and Census Block Group Data, 2020 [Digital data]. U.S. Department of Commerce, Washington, D.C.

U.S. Geological Survey (USGS). (2018). National Elevation Dataset (NED), 1/3 Arc-Second [Digital data]. U.S. Geological Survey, Reston, VA. https://nationalmap.gov/elevation.html

UNISDR. (2015). Making development sustainable: The future of disaster risk management (Global Assessment Report on Disaster Risk Reduction 2015). United Nations Office for Disaster Risk Reduction.

Wachinger, G., Renn, O., Begg, C., & Kuhlicke, C. (2013). The risk perception paradox—Implications for governance and communication of natural hazards. Risk Analysis, 33(6), 1049–1065.

Wang, Z., Mao, D., Wu, J., & Xu, J. (2019). Modeling flood risk communication processes using agent-based modeling. International Journal of Disaster Risk Science, 10(3), 417–432.

Wilensky, U. (1999). NetLogo. Center for Connected Learning and Computer-Based Modeling, Northwestern University. Evanston, IL. http://ccl.northwestern.edu/netlogo/

Wilensky, U., & Rand, W. (2015). An introduction to agent-based modeling: Modeling natural, social, and engineered complex systems with NetLogo. MIT Press.

Wing, O. E. J., Pinter, N., Bates, P. D., & Kousky, C. (2022). New insights into the US flood exposure from high-resolution population data. Nature Communications, 13(1), 1–10.

Yeşilköy, S., Baydaroğlu, Ö., Singh, N., Sermet, Y., & Demir, I. (2024). A contemporary systematic review of cyberinfrastructure systems and applications for flood and drought data analytics and communication. Environmental Research Communications, 6(10), 102003.

Zhang, H., Chen, K., Xu, S., & Xie, H. (2020). Agent-based modeling of flood evacuation with consideration of social perception and shelter accessibility. Sustainability, 12(12), 5038.